Structural, electronic, and vibrational properties of diamond (100), (111), and (110) surfaces from *ab initio* calculations

Dominic R. Alfonso
Department of Chemistry and Condensed Matter and Surface Sciences Program, Ohio University, Athens, Ohio 45701-2979

David A. Drabold and Sergio E. Ulloa
Department of Physics and Astronomy and Condensed Matter and Surface Sciences Program, Ohio University, Athens, Ohio 45701-2979

(Received 3 January 1995)

Using a first-principles technique, we calculate the structural, electronic, and vibrational properties of the (100), (111), and (110) surfaces of diamond. Stable (2×1) and Pandey chain reconstruction were found for the bare (100) and (111) surfaces, respectively. The surface zigzag chain of the (110) face is buckled and accompanied by a small charge transfer between the surface atoms. Hydrogen adsorption on these surfaces is energetically favorable. The electronic structures of the unhydrogenated surfaces show gap states which disappear upon termination of the surfaces with H atoms. Simulated scanning tunneling microscopy images are also presented. Vibrational modes involving excitations of the surfaces dimers and chains were identified for the clean surfaces, while phonon modes associated with H stretching and H bending motions were found for the hydrogenated surfaces.

I. INTRODUCTION

From both basic science and technological perspective, investigations of the diamond surfaces are of great interest. Diamond films are potential materials for commercial applications such as machine tools, optical coatings, and high temperature electronics, due to its properties which includes extreme hardness, high thermal conductivity, and chemical inertness.[1] Recent attempts have been made in the area of fabricating diamond-Si and diamond-transition metal interfaces.[2] A thorough understanding of these materials and its surfaces at the atomistic level are, therefore, important. Moreover, there is a growing demand to accurately understand the physical properties of the various low-index faces of diamond surfaces with the motivation of investigating its similarities and differences. The diamond (100), (111), and (110) surfaces are typical growth planes for hydrocarbon precursors deposited using chemical vapor deposition (CVD) processes. Scanning electron microscopy studies revealed that only the (100) and (111) faces are found to occur predominantly in polycrystalline diamond films suggesting that the (110) face is the fastest growing plane.[3] Geis and Chu *et al.* found that the relative growth rates is in the order (100) > (111) > (110).[4] Hence, a systematic understanding of its structural characteristics may not only play a role in determining the morphology of these systems, but may also be a relevant first step in understanding the relative growth rates and dynamics of the film on these surfaces.

The diamond surfaces have been the focus of various experimental investigations.[5] The C(100) surface has two dangling bonds per bulk-terminated surface atom, while C(111) and C(110) have single dangling bonds per surface atom. Lurie and Wilson observed a (1×1) low energy electron diffraction (LEED) patterns for the C(100), C(111), and C(110) surfaces.[6] At elevated temperature (~ 1300 K), they found (2×1) patterns for the C(100) and C(111) surfaces, which are indicative of (2×1) surface reconstruction. Reconstruction on the C(100) and C(111) surfaces is also suggested by scanning tunneling microscopy (STM), and independent spectroscopic and ion-scattering studies.[7–9] Chemical vapor deposition diamond films are usually grown in a saturated H atom environment. H atoms are postulated to be generators of radical sites and destabilizer of the graphitic phase on the growing substrate. Recent high resolution electron energy loss spectroscopy (HREELS) studies indicate that the C(100) and C(111) surfaces are hydrogen terminated.[10,11] Moreover, electron stimulated desorption time-of-flight measurements, vibrational investigations, and other experimental studies showed that the C(100), C(111), and C(110) surfaces are covered with hydrogen atoms.[12–15] From photoemission spectroscopy, the hydrogenated (100), (111), and (110) surfaces are found to have no states in the gap.[14–16]

The diamond surfaces have been the subject of numerous theoretical studies using semiempirical and first-principles methods.[17–21] Iarlori *et al.* employed Car-Parinello molecular dynamics (MD) simulations to characterize the (2×1) reconstruction on the C(111) surface.[17] Jing and Whitten used an *ab initio* cluster method to investigate the reconstruction on the clean C(100) surfaces.[18] Yang *et al.* investigated the relaxed geometries and electronic density of states of the C(100) surface using a local basis, Harris functional first-principles molecular dynamics technique.[19]

Recently, Davidson and Pickett studied the band structure, total energy, and structural properties of the C(100), C(111), and C(110) surfaces by semiempirical tight-binding method.[20] Despite the enormous experimental research efforts, there are few systematic studies of the (100), (111), and (110) surfaces of diamond, using a reliable first-principles technique. As implied above, an important prerequisite in modeling growth is to understand the properties of these surfaces. There are also virtually no first-principles studies of the C(110) surface. Not only is this face found to be the fastest growing plane during CVD growth, but it was also predicted that migration of H and halogens on this surface is sufficiently fast to compete with gas phase reactions and hence, may play a role in diamond CVD.[22] It is of utmost interest, therefore, to study this surface.

Another key surface probe is STM. A close connection between theory and experiment is desirable here as well. For example, STM observations performed on the (100) surface of grown diamond epitaxial film reveal the presence of dimer rows.[7,23] To our knowledge, there is no first-principles simulation of the STM images that will assist in the interpretation of these and other findings. The vibrational properties are also of interest. Recently, HREELS experiments confirmed the presence of phonon modes intrinsic to the diamond surfaces.[10,11] While the use of these surface-vibration probes to investigate diamond surfaces is receiving increasing attention, the only previous work has been a preliminary report on the diamond (100) surface from our group.[24] Current analysis of the measured vibrational spectra of the diamond surfaces relies heavily on information from gas phase molecular vibrational frequency data and scaled phonon frequencies for similarly reconstructed silicon surfaces. These schemes, while having some utility in interpreting experimental results, are however limited, since surface vibrational features intrinsic to the diamond surfaces would not be included in this approach. A first effort in shedding light on the measured vibrational data is our recent theoretical phonon modes studies of C(100) surfaces, using first-principles techniques.[24] The excellent agreement of our findings with experiments has encouraged us to extend our phonon mode calculations to the (111) and the (110) surfaces and eventually make a detailed comparison of the vibrational properties among the different diamond surfaces.

In this paper, we present thorough theoretical studies of the C(100), C(111), and C(110) surfaces, using accurate *ab initio* methods, based on density functional theory. Initial efforts using this method in the characterization of diamond (100) surfaces yielded results in excellent agreement with experiments.[19,24] Our objective in this paper is to present a comprehensive report of the structural, electronic, and vibrational properties of the clean and hydrogenated diamond (100), (111), and (110) surfaces. To our knowledge, this is the first systematic comparison between the properties of the various diamond surfaces, using a reliable first-principles technique.

The methodology is discussed in Sec. II, while the results of the calculations are presented and discussed in Sec. III.

II. METHODOLOGY

A. Molecular dynamics

The present calculation employs the method developed by Sankey *et al.*,[25] which is a first-principles molecular dynamics simulations based on density functional theory. Its suitability for covalent systems such as C and Si is well proven and documented.[25–27] In particular, the method has been previously applied to the diamond (100) reconstruction and yielded results in good agreement with self-consistent plane-wave calculations.[19,24] Moreover, application of this method to determine the phonon modes of the C(100) surfaces gave results, which reproduce the main features of the experimental phonon spectra.[24] Key features of this approach include (1) a spin unpolarized non-self-consistent version of the density functional theory using the Harris functional, and the local density approximation (LDA);[28] (2) nonlocal, norm conserving pseudopotentials of Bachelet-Hamman-Schlüter type;[29] (3) a minimal basis set where the local orbitals (one s- and three p-like functions per site) have compact support, reflecting a confinement boundary condition (orbital confinement radii for C and H are 4.1 and 3.8 a.u., respectively).[25] The LDA exchange correlation term assumes the Ceperley-Alder form as parametrized by Perdew and Zunger.[30,31] Transferability has been carefully investigated, and excellent agreement is obtained with the self-consistent plane-wave phase diagram.[32]

The diamond substrates were modeled as slabs with periodic boundary conditions in the two directions parallel to the surface and hence, the models are effectively infinite in two dimensions. For the flat C(100), C(111), and C(110) (clean and hydrogen terminated) surfaces, we utilized large slabs consisting of 10 C layers and having 8 C atoms per layer. The bottom C layer of these slabs are terminated with H atoms. To sample the electronic Brillouin zone of these large supercells, two special Monkhorst-Pack $\vec{k}$ points were employed.[33] An important advantage of a *local* basis set is that no artificial periodicity (as encountered with plane waves) is required in the direction normal to the slab. The equilibrium structures of all our simulation systems were achieved using a dynamical quenching technique.[26] The atoms are allowed to respond to internal forces and are accelerated accordingly. The resulting kinetic energy of the system increases as the atoms accelerate, until it reaches a maximum. The kinetic energy of the system is then removed by setting all the velocities equal to zero at one time, after which the atoms are allowed to accelerate again and the quenching process is repeated. To reduce computational demands, the slab is first relaxed using a semiclassical dynamics based on Tersoff-Brenner semiempirical potential expressions for the hydrocarbon system.[34] We then take these approximately optimized structures and further relax them using *ab initio* scheme until the force experienced by each atom is less than 0.02 eV/Å. This approach of initially relaxing the slab using the semiempirical potential and finally obtaining the minimum energy configurations by first-principles MD simulations has been applied successfully in previous studies and verified for appropriate convergence.[24,35]

B. Electronic structure

We also performed a set of calculations to determine the surface electronic band structures of the diamond substrates. Instead of using ten slabs with eight carbons per layer (which we employed to evaluate the structural properties, phonons, and simulated STM images of the diamond surfaces), we used instead 16 C layer deep simulation systems that contain two atoms per layer with inversion symmetry about a point in the center of the slab. Notice that the slabs were arranged so that both the upper and lower layers are considered surfaces, and therefore, a deeper simulation system is used to faithfully model the bulk relaxation. We then search for the most stable structure with the first-principles technique we just described, using 32 special $\vec{k}$ points to sample the primitive cell surface Brillouin zone (SBZ).[33] All the atoms were allowed to relax except for the middle two C layers. After optimization, we found that each 32 C slabs with improved SBZ sampling did yield surfaces and bulk structures with similar qualitative features and slight quantitative changes when compared against the bigger slab.

To make contact with available experimental STM data, we compute surfaces of constant local charge density, using a given energy interval typically centered at occupied energy bands near the Fermi level. Simulating STM images in this fashion follows the work by Tersoff and Hamann,[36] which states that the contribution of a given state to the STM tunneling current is proportional to the square of its wave function. By summing the contributions in the appropriate interval, one can approximately calculate the STM profiles measured at constant tunneling current.

C. Surface phonon modes

The vibrational properties are obtained by construction and diagonalization of the dynamical matrix $\phi^{ij}_{\alpha\beta}$, yielding the phonon eigenvalues and eigenvectors. $\phi^{ij}_{\alpha\beta}$ is obtained by displacing an atom i from its equilibrium position by 0.03 Å in the direction α and calculating the forces acting on atom j in the direction β. Here, $\alpha=(x,y,z)$ and $i=1,...,N$, where N is the total number of atoms. To allow a more direct comparison with experiment, we have calculated the projected *surface* phonon density of states:

$$\rho_{\text{surface}}(\omega)=\sum_{\nu n}\delta(\omega-\omega_n)|\langle\chi_n\mid\nu\rangle|^2, \quad (1)$$

where n are the eigenmodes, while ν are the x,y, and z components of the eigenmodes of the projected top layer atoms, and $\mid\chi_n\rangle$ is the nth eigenvector of the dynamical matrix. Physically, Eq. (1) is the local contribution to the vibrational density of states from the projected surface atoms.

III. RESULTS AND DISCUSSION

A. Diamond (111) surface

1. Structures

The as-polished C(111) surface was determined to have the ideal (111)-(1×1) bulk-terminated structure as indicated by LEED and He scattering experiments.[6,12,37] Reconstruction from (1×1) to the stable Pandey (2×1) chain structure occurs as the substrate is annealed above 1000 °C.[10,12] Moreover, experimental studies have shown that upon exposure of the (111)-(2×1) Pandey chain reconstructed surface to H atoms, it transforms to a hydrogenated phase, where the carbon atoms have the characteristics of the bulk.[12,38] We report here the characterization of the various clean and H-terminated C(111) substrates, using sufficiently large slabs to model the surface. The surface structure of the bulk-terminated C(111) surface has atoms that are threefold coordinated with atoms on the subsurface layer, and contain dangling bonds normal to the surface plane. The top layers of the C(111)-(2×1) slab were similar to the structure reported by Pandey, where the surface (2×1) reconstruction comprised of π bonded chains in the first upper two layers.[39] To model the hydrogenated bulk terminated and Pandey reconstructed surfaces, the model slabs are terminated by hydrogen atoms (one per C atom on surface layer). All the atoms in the simulation systems were then allowed to relax (except for the bottom C layer) to their minimum energy configurations, using the minimization technique described previously. From here on, we will often refer to the bare bulk-terminated and Pandey reconstructed surfaces as C(111)-(1×1) and C(111)-(2×1) surfaces, respectively. The H-terminated phase of these surfaces, on the other hand, will be denoted as C(111)-(1×1)H and C(111)-(2×1)H, respectively. Diagrams of the various types of (111) surfaces considered in this work are illustrated in Fig. 1.

Table I summarizes the result of the relaxation of the model clean and hydrogenated diamond (111) surfaces. Upon relaxation, the first layer (topmost) carbon atoms of the bulk terminated surface sink in to the slab by an average inward displacement of ~ 0.22 Å. We also find a decrease in the bondlength between the first two layers (Δr_{12}) by –5.1%. Our result is consistent with *ab initio* calculations of Vanderbilt and Louie,[40] who found a Δr_{12} of –3.1% and Stumpf and Marcus,[41] who reported a Δr_{12} of –4.0%. The C-C bondlengths between the carbons on the second and third layer, Δr_{23}, increase by 7.0%. The equilibrated (111) Pandey chain reconstructed surface has zigzag chains on the first layer with average bondlength of 1.44 Å, which is comparable to graphite. We found no buckling of the dimerized surface π bonded chain. The chain on the second layer has bondlengths equal to 1.55 Å, slightly smaller than the C-C diamond value of 1.57 Å. In agreement with other first-principles calculations and a number of experimental studies, the (111) Pandey chain reconstruction is energetically favored. We find the reconstruction to be favored by about 0.63 eV/(surface atom) versus the

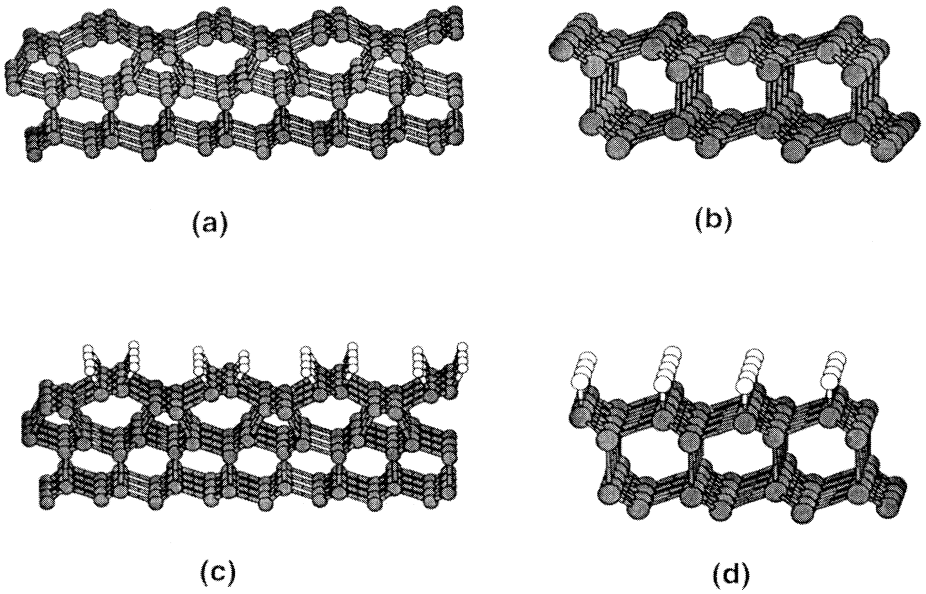

FIG. 1. Diagrams (side view) of (a) Pandey chain reconstructed, (b) bulk terminated, (c) hydrogenated Pandey chain reconstructed, and (d) hydrogenated bulk-terminated (111) surfaces of diamond. Carbon atoms appear shaded, hydrogen atoms white.

bulk-terminated structure.

Numerous studies have suggested that one of the roles of the H atoms (which is present during typical CVD diamond growth) is to destabilize sp^2 bonding configuration on the growing diamond surface.[1,2,5] In the present work, we studied CH bond formation on both (1×1) and (2×1) C(111) surfaces. Table I summarizes the result of the relaxation of the hydrogenated (111) phases. The relaxed Pandey chain reconstructed surface has a C-H bondlength of 1.19 Å, where the H atoms are tilted from the surface normal by about 28°. The formation of CH bonds increases the C-C chain bondlength to 1.61 Å. For the bulk-terminated case, the C-H bondlength is also 1.19 Å, with the C-H bond pointing normal to the surface plane. Our calculated C-H bondlength is comparable to the *ab initio* value of 1.12 Å from Zhu and Louie,[42] and 1.1255 Å from Stumpf and Marcus.[41] The formation of C-H bonds increases the bondlength between the first and second layer carbons to 1.55 Å, with respect to the clean surface.

The present work predicts energies of −0.52 eV/(surface atom) and −0.22 eV/(surface atom) for the hydrogenated and bulk terminated and hydrogenated Pandey chain reconstructed surfaces, respectively, with respect to the bare Pandey chain reconstructed surface, plus gas phase H_2 molecules. Our results, therefore, correctly predict that hydrogen adsorption is energetically favorable, and that hydrogen adsorption on the bulk-terminated (1×1) surface is the preferred structure over the hydrogenated (2×1) Pandey chain reconstruction.

2. *Electronic properties*

Figure 2 shows the surface electronic level structure of the clean (111) surface yielding gap states with predominantly p_z character upon inspection of the eigenvectors associated with these levels. The origin of the states in the band gap is determined by performing localized charge calculations.[43] From inspection of the localized eigenvalues in the band gap, we find that the sp^2 surface

TABLE I. Structural properties for the various relaxed (111) surfaces of diamond. See text for description of Δr_{12} and Δr_{23}. $r_{1(C-C)}$ and $r_{2(C-C)}$ are the C-C bondlength of the first and second layer chains of the C(111)-(2×1) surface, respectively. r_{C-H} and Θ_{CH} are the surface CH bond distance and its tilt, with respect to the surface normal. The values in parentheses are results from other first-principles calculations.

	C(111)-(1×1)	C(111)-(1×1)H	C(111)-(2×1)	C(111)-(2×1)H
Δr_{12}(%)	−5.1 (−3.1[a], −4.0[b])	∼ 1		
Δr_{23}(%)	+7.0	−3.0		
$r_{1(C-C)}$ (Å)			1.44 (1.47[b], 1.44[c])	1.61
$r_{2(C-C)}$ (Å)			1.56	1.59
$r_{(C-H)}$ (Å)		1.19		1.19
Θ_{CH} (deg)		0		28

[a]Reference 40.
[b]Reference 41.
[c]Reference 17.

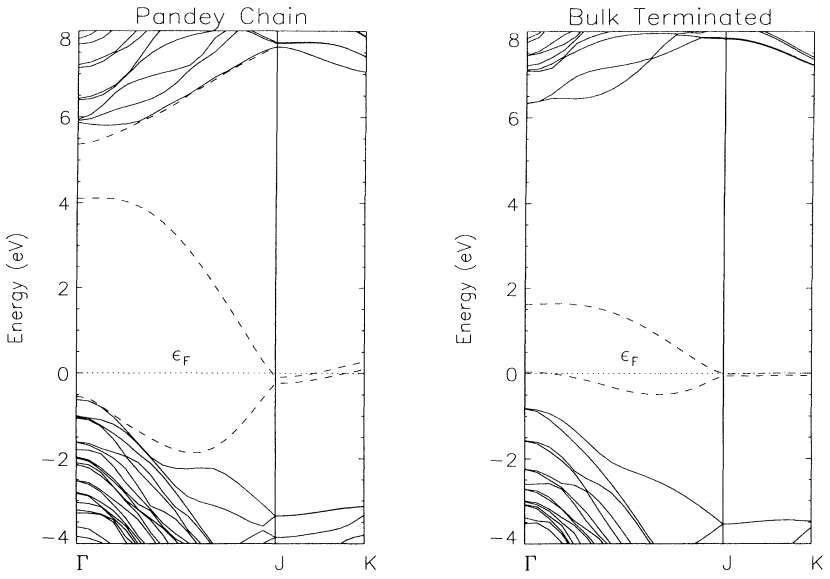

FIG. 2. Band structures for the clean Pandey chain reconstructed and bulk-terminated (111) surfaces of diamond. Dotted lines refer to the Fermi level, while broken lines denote gap states. $\Gamma \rightarrow J$ is along the chain direction, $J \rightarrow K$ is perpendicular.

atoms were the sites in which the charge is most strongly localized. These undercoordinated atoms, therefore, are responsible for the gap states.

The band structure of the relaxed C(111)-(2×1) surface yielded features that are in excellent agreement with previous *ab initio* investigations. At the Γ point, we see a splitting of ~5 eV between the occupied and unoccupied states, compared with the splitting of ~4.8 and ~3 eV, obtained by Vanderbilt and Louie and Iarlori *et al.*, respectively.[40,17] The surface states in these calculations and our work result to be nearly degenerate with the valence band edge at the zone center. We find an additional gap state between the conduction band and the unoccupied dangling bond state as did Vanderbilt and Louie for the (2×1) reconstruction. This surface band in the vicinity of the conduction band edge has localized charge on the second layer chain atoms. From the zone edge to the J direction (along the first layer chain), the surface states become nearly degenerate. Similar to the result of Vanderbilt and Louie, we calculated a more dispersive band increasing in energy in the J-K direction, which is perpendicular to the surface chains (the higher surface state band crosses the Fermi level, indicating that the surface is metallic). This dispersion indicates that the neighboring chains interact and the inequivalence of the surface atoms making up the chain gives rise to a splitting, as pointed out in Ref. 40. The salient features of the band structure of C(111)-(2×1) are qualitatively similar to those obtained with angle-resolved ultraviolet photoemission spectroscopy and angle-resolved two-photon spectroscopy measurements.[9,44] These experiments show the presence of occupied and unoccupied surface states having p_z character, as we find.

The dangling bonds on the C(111)-(1×1) surface yield occupied and unoccupied states in the band gap, as shown in the right panel of Fig. 2. At the Γ point, the occupied level is about 0.8 eV above the valence band maximum and the splitting between the occupied and empty states is about 1.6 eV. Vanderbilt and Louie calculated an occupied level which is ~ 2 eV above the conduction band edge at the Γ point. They, however, found a much smaller splitting between the occupied and empty states, compared to our results. From the zone edge and along the J and K directions (along one-half of the longer reciprocal lattice vector and the corner of the SBZ, respectively), the higher energy state crosses the Fermi level, suggesting that the clean bulk-terminated surface is metallic.

Shown in Fig. 3 are the band structure of the corresponding hydrogenated phases of both the C(111)-(1×1) and C(111)-(2×1) surfaces. Both panels show no states in the gap resulting from the removal of the dangling bonds by formation of CH bonds. Photoemission experiments on the C(111) surface reveal that the (1×1) phase has no surface states in the gap.[15] The present work indicates that H adsorption removes gap states and therefore suggests that the C(111)-(1×1) surface measured in Ref. 15 is fully H terminated. We would like to note in passing that our calculated band gaps at the Γ point for all the hydrogenated surfaces considered in this work overestimated the band gap of bulk diamond by about 0.5 – 1 eV. Only inclusion of d-like orbitals in our basis sets and more accurate treatment of correlation effects could remedy this discrepancy.

Busmann *et al.* performed an STM measurement on the as-grown (111) face of their polycrystalline diamond film.[45] The STM images show regions having corrugated hexagonal pattern with characteristic spot-spot distance of about 2.5 Å . The sixfold symmetry shown was attributed to the (1×1) structure. They also observed other characteristic images where rows appear, with angular behavior consistent with Pandey's C(111)-(2×1) chain. We simulate the STM images of the hydrogenated bulk terminated C(111)-(1×1) and clean Pandey chain reconstructed (111)-(2×1) surfaces — the more energetically stable hydrogenated and bare (111) surfaces, respectively. Figure 4(a) shows constant-height contours of the constant density surface of the H-terminated (1×1)

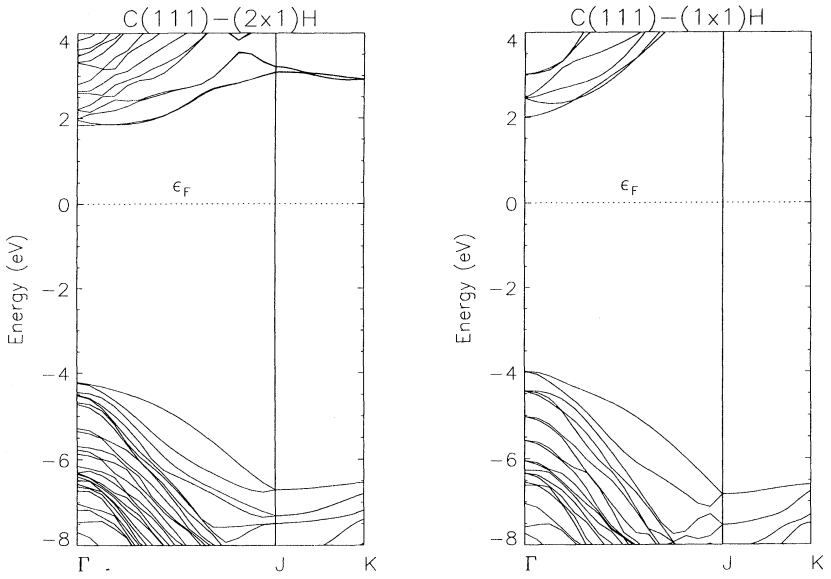

FIG. 3. Band structures for the hydrogenated Pandey chain reconstructed and bulk-terminated (111) surfaces of diamond. $\Gamma \rightarrow J$ is along the chain direction, $J \rightarrow K$ is perpendicular.

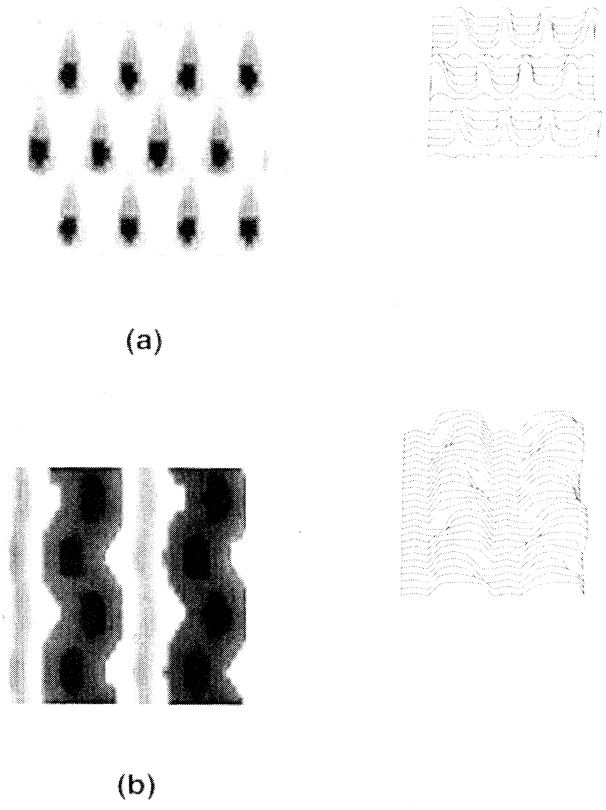

FIG. 4. Simulated STM images of the (a) hydrogenated bulk terminated and (b) Pandey chain (2×1) reconstructed (111) surfaces of diamond. Plots are drawn at isodensity $\rho \sim 0.01$ e/Å^3.

surface. This plot is obtained using an energy interval of 0.1 eV, at the top of the valence band and can be compared with the result in Ref. 45. The isodensity surface for the C(111)-(1×1)H substrate shows features along the CH bonds, with a maximum appearing along the direction of the CH bond axis. The calculated image shows a hexagonal pattern, with nearly perfect sixfold symmetry. The distance between the maxima is about about 2.3 Å, slightly smaller than the characteristic spot-spot distance (2.5 Å) observed in the experiment. Clearly, the (1×1)-like feature observed in Ref. 45 are due to the hydrogenated (1×1) bulk-terminated structure.

Figure 4(b) shows the simulated STM image of the clean (2×1) Pandey chain reconstructed surface. The plot was obtained using an energy interval of about 0.2 eV centered at 1.2 eV below the Fermi energy near the top of the valence band. Notice that the isodensity maxima appear on the surface carbons and a minimum appears along the zigzag chain. Features associated with the subsurface chains are slightly visible, and correspond to the deeper minimum "valley" between adjacent zigzag chains. This feature along the surface chain may correspond to the rows observed in the experiment. The present work, therefore, suggests that the two likeliest phases on the as-grown diamond (111) surfaces are the Pandey chains and hydrogenated bulk structures. The STM measurements with higher profile definition will be desirable in order to allow direct imaging of the finer structure on the structure on the different surfaces here. We did not calculate constant density surfaces for the C(111)-(1×1) and C(111)-(2×1)H substrates since our previous energetics argument together with STM and HREELS experiments suggest that these particular phases of diamond are highly unlikely to be present in an as-grown (111) face of diamond film.[10,45]

3. *Phonons*

In this section, we discuss the vibrational modes associated with the (111) surfaces of diamond. We have only calculated the phonon spectra of the most stable bare and hydrogenated phases of the (111) surfaces — the C(111)-(2×1) and C(111)-(1×1)H surfaces, respectively. Figure 5 shows the surface vibrational density of states (VDOS) of these surfaces. The (111) phonon spectrum was obtained by projecting out the VDOS of the three topmost C layers of the model slab and including the surface H atoms in the case of the H-terminated sample. We found that relevant surface features were confined mainly to the upper layers that we consider by performing a comparison between the layer-resolved VDOS and the corresponding bulk results. The calculated vibrational spectra were broadened using a Lorentzian of width 40 cm^{-1}, to match the experimental resolution of the HREEL spectrometer employed in Ref. 10.

The C(111)-(2×1) spectrum has features below $\sim$ 1500 cm^{-1} and has two main broadbands between $\sim$ 500–900 cm^{-1} and $\sim$ 900–1500 cm^{-1}. We have identified modes associated with the excitations of the first and second layer zigzag chains. The region between $\sim$ 400–1000 cm^{-1} is dominated by excitations of these chains normal to the surface plane, while several modes, due to in-plane excitations of the chains are found in the region $\sim$ 1100–1400 cm^{-1}. Table II lists some of the main surface phonon modes, which were identified as rocking, bouncing, and dimer motion of the chain fragments (diagrammatic representations of the eigenvectors associated with some of these modes are found in Fig. 6). We identified bouncing modes that are nearly localized to the first and second layer chains (418 and 837 cm^{-1}, respectively). In particular, the bouncing vibration at 837 cm^{-1} is associated with the in-phase motion of the entire surface chain fragments, with respect to the subsurface chains. The rocking vibration involves out-of-phase surface normal oscillations of the atoms making up the chain fragments. Splitting of the rocking motion of the surface chain are found involving symmetric (624 cm^{-1}) and antisymmetric (633 cm^{-1}) modes, where the adjacent chains vibrate in phase and 180° out of phase, respectively. The antisymmetric motion is slightly higher in energy, due to the more pronounced excitation on the second layer chains. If one imagines the chain fragments to be weakly coupled adsorbed polymers, then the rocking and bouncing modes of the surface zigzag chains correspond to the torsional or transverse vibration of the polymer, which has zero energy for a free chain. These motions, however, are considered hindered and acquire a finite frequency, since the chain is coordinated to the subsurface atoms. The second layer chain, on the other hand, is relatively "stiffer," due to its higher coordination number as compared to the first layer chain. This explains why the bouncing and rocking vibration of the subsurface chain have higher energy than its counterpart motion on the surface chain. The dimer modes at 1117 and 1258 cm^{-1} have a characteristic vibrational motion along the first layer or second layer chain fragments, which has the effect of dynamically modifying the dimerization of the C-C bonds of the chain. Two versions of these modes exist — the lower energy, corresponds to a vibration where the first and second layer chains move in phase, while the second version at 1258 cm^{-1} involves out of phase motion of the two topmost layer chains [see Figs. 6(f) and 6(g), respectively]. The out-of-phase vibration has higher energy, because of the more pronounced lattice excitation associated with this mode.

Recently, Lee and Apai employed HREELS to measure the vibrational properties of the C(111)-(2×1) surface.[10] The HREELS spectrum yielded three phonon bands at 740, 970, and 1235 cm^{-1}. These features are broadly reproduced in our theoretical phonon spectrum and estimated to fall in the energy regions of 500–800 cm^{-1}, and 900–1100 and 1100–1300 cm^{-1}. Their 970 cm^{-1} band appears to correspond to our 982 cm^{-1}, which involves second layer zigzag chain rocking motion [see Fig. 6(c)]. The 1235 cm^{-1} band that they identify may correspond to a superposition of dimer modes discussed above and illustrated in Figs. 6(f) and 6(g). The predicted 624 cm^{-1} (in-phase rocking motion of the surface chain) or 837 cm^{-1} (bouncing vibration of the second layer chain) probably correspond to their 740 cm^{-1} feature. We should note that the calculated spectra for all the diamond surfaces considered in this work yielded more spectral features than the experimental HREELS spectra since the calculated VDOS are not limited by coupling selection rules of the surface to the probe. Moreover, our methodology is not constrained by possible instrumental energy resolution (although the broadening introduced mimics this) and therefore, all surface phonon modes are "detected." Notice, however, the we cannot reliably study the low frequency region of the spectrum because of finite size

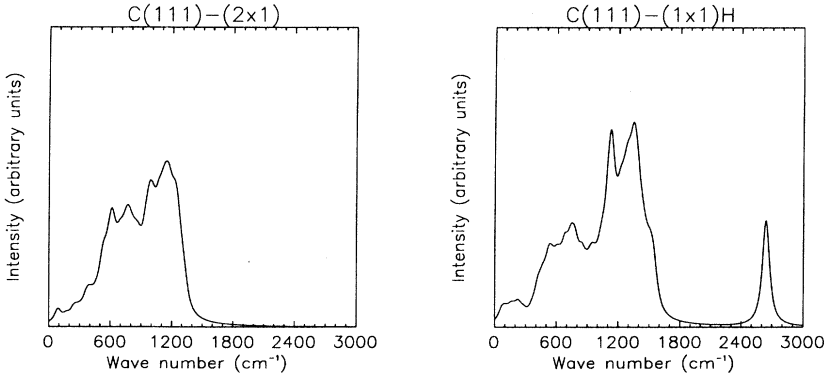

FIG. 5. Vibrational density of states of the bare Pandey chain reconstructed and hydrogenated bulk-terminated (111) surfaces of diamond.

TABLE II. Sample calculated frequencies and corresponding description of surface-vibrational modes in C(111)-(2×1) and C(111)-(1×1)H surfaces. The phase refers to the motion of the neighboring zigzag chain fragments.

Frequency (cm^{-1})	Description	Fig. 6
	C(111)-(2×1)	
624	surface chain rocking (in phase)	a
633	surface chain rocking (out of phase)	b
982	subsurface chain rocking (out of phase)	c
418	surface chain bounce (in phase)	d
837	subsurface chain bounce (in phase)	e
1117, 1258	dimer mode (see text)	f, g
	C(111)-(1×1)H	
2664	CH stretch	h
~ 1100-1550	CH bend	i
1010	breathing mode (see text)	j

effects introduced by the finite model slabs that we employ. This low frequency region (typically below ~ 300 cm^{-1}), however, is generally experimentally inaccessible to surface-vibration probes.[46]

The calculated VDOS for the C(111)-(1×1)H surface is shown in Fig. 5 (right panel), and has broadbands below ~ 1550 cm^{-1} and an intense feature centered at 2664 cm^{-1}. Phonon modes associated with surface C-H stretch and bend vibrations are identified and summarized in Table II. The highest band at 2664 cm^{-1} is identified as symmetric stretch of the C-H bonds. The region ~ 1100–1550 cm^{-1} is dominated by CH bending vibrations, which are coupled to lattice excitations. An example of these modes is illustrated in Fig. 6(i), where CH fragments undergo a bending motion in phase with neighbors. Below 1100 cm^{-1}, we find excitations that are nearly localized to the few topmost carbon layers. A very interesting mode is the "breathing" mode at 1010 cm^{-1} [see Fig. 6(j)]. This mode has the characteristic of modifying the interplanar spacing in the carbon layers, since the oscillation of the first layer carbons is out of phase with respect to the second layer. Previous experimental investigations on the vibrational properties of the H-covered C(111) surface revealed phonon bands at 2900–2930 cm^{-1} and near 1300 cm^{-1},[47] which were attributed to surface H stretching and bending vibrations, respectively. Waclawski *et al.* observed peaks at 2900 and 1290 cm^{-1}, for the H-exposed C(111) surface from HREELS measurements.[48] These features were assigned to C-H stretches and bends, respectively. Using HREELS, Sun *et al.* observed peaks at 1240 and 2920 cm^{-1} for their faceted (111) polycrystalline diamond film and assigned them to H bend and stretch motion, respectively.[49] Lee and Apai reported a peak centered at about 2930 cm^{-1}, which they assigned to CH_x ($x = 1 - 3$) stretching vibrations.[10] Moreover, a broad peak from 680 to 1670 cm^{-1} was found and assigned to CH_x deformation modes. Recent HREELS experiment by Aizawa *et al.* on their as-grown C(111) surface indicated bands in the region ~ 1000–1600 cm^{-1} and near 2839 cm^{-1}, which were attributed to adsorbed CH_3 bending and stretching vibrations, respectively.[11] Our calculations predict surface H related modes, such as H stretch and H bend modes, for the C(111)-(1×1)H substrate consistent with these experimental results.

B. Diamond (100) surface

1. *Structures*

The ideal diamond (100)-(1×1) surface is known to undergo reconstruction to form a dimerized (100)-(2×1) structure.[14,50] To model this structure, the 10 C layer thick slab was allowed to relax (except for the bottom C layer) and self-reconstruct into the (2×1) dimerized surface [a diagram of the C(100)-(2×1) surface is illustrated in Fig. 7(a)]. The hydrogenated (100) surface is also of interest since experimentally, H atoms are present in abundance, during the film growth and could passivate the dangling bonds present in each surface carbon. The first *ab initio* calculation on the diamond (100) sur-

TABLE III. Structural properties for the relaxed (100) surfaces of diamond. r_{C-C} and r_{C-H} denote the dimer bondlength and surface C-H bond, respectively. Δd_{12} is the percent change in the first interplanar spacing. Θ_{CH} is the tilt of the surface C-H bond from the surface normal. Δh_3 and Δh_4 are the buckling amplitudes of the C atoms in the third and fourth C layer, respectively. The value in parentheses refers to results from other first-principles calculations.

	C(100)-(2×1)	C(100)-(2×1)H
$r_{(C-C)}$ (Å)	1.36 (1.39[a], 1.401/1.508[b])	1.62
$r_{(C-H)}$ (Å)		1.18
Δd_{12} (%)	−24	−5
Δh_3 (Å)	0.13	0.10
Δh_4 (Å)	0.25	0.17
Θ_{CH} (deg)		24

[a]Reference 51.
[b]Reference 18.

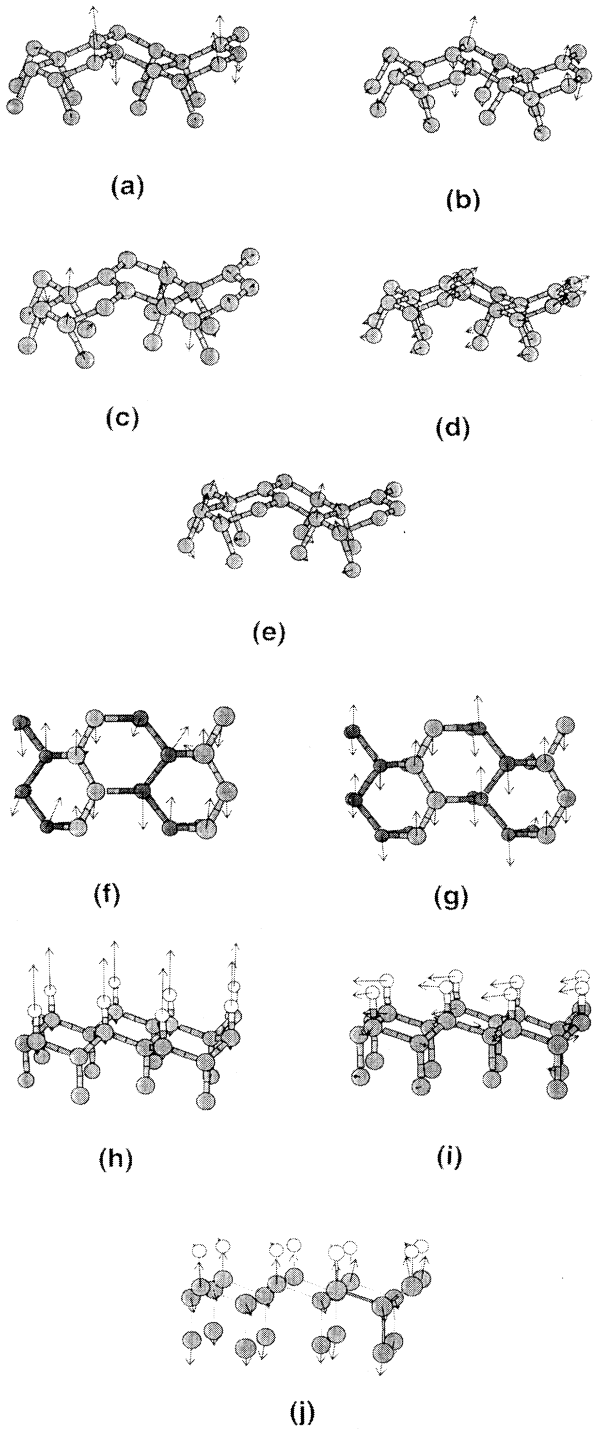

FIG. 6. Eigenvector representations of some of the phonon modes associated with the (111) surfaces of diamond for the Pandey chain reconstructed surface and hydrogenated bulk-terminated surfaces: (a) surface chain rocking (in phase), (b) surface chain rocking (out of phase), (c) subsurface chain rocking (out of phase), (d) surface chain bounce (in phase), (e) subsurface chain bounce (in phase), (f) dimer mode (in phase), (g) dimer mode (out of phase), (h) CH stretch, (i) CH bend (in phase), and (j) breathing mode. Carbon atoms appear shaded, hydrogen atoms white. Arrows show amplitudes for each atom in each mode.

face was carried out by Yang *et al.*, using the present method and a slightly different basis set.[19] The structural and electronic results reported here are in close accord with that calculation, except for insignificant differences, due to the improved basis set employed in this paper. It has been established from previous theoretical works[20,34] that the monohydride diamond (100)-(2×1) surface [C(100)-(2×1)H] is the more energetically favorable structure compared to the clean surface. To model this surface, we terminate each dimer carbon of our clean (100)-(2×1) slab with hydrogen atoms [see Fig. 7(b) for a diagrammatic representation]. With the bottom C layer fixed, the H-terminated slab was allowed to relax to their minimum energy configurations employing the minimization scheme described above.

Table III summarizes the structural parameters we obtained for the clean and monohydride (100)-(2×1) surfaces. The predicted equilibrium structures contained rows of symmetric dimers as a result of rebonding in the surface. The CC dimer bondlength for the clean surface is 1.36 Å, which lies between the CC single bondlength of 1.54 Å and CC double bondlength of 1.34 Å in most nonconjugated molecules.[52] This indicates that the clean surface CC dimer bonds are intermediate between single and double bonds. The fact that the CC dimer bondlength is slightly bigger than a typical C=C bond distance is not surprising, due to the strain imposed by the lattice. Moreover, the rebonding of the surface atoms gives rise to the relaxation of atoms in the subsurface layers. The first interplanar spacing is contracted 24%, with respect to the bulk interplanar distance. The buckling amplitudes (relative difference in the z coordinates of adjacent

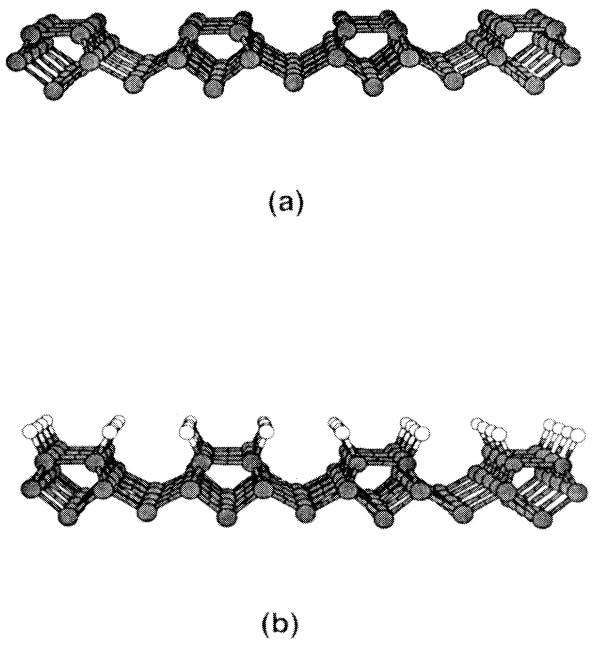

FIG. 7. Diagrams (side view) of (a) clean and (b) hydrogenated (2×1) reconstructed (100) surfaces of diamond. Carbon atoms appear shaded, hydrogen atoms white.

carbon atoms) on the third and fourth layers are about 0.13 and 0.25 Å, respectively.

The dimer CC bond distance for the monohydride phase is 1.62 Å, larger than the diamond CC bulk bondlength of 1.57 Å. The increase in the bondlength of the dimer can be attributed to the increase in coordination number as a result of the formation of CH bonds. The CH bond distance is 1.18 Å and tilted by about 24° away from the other H bonded to the same dimer. We observe less subsurface relaxations, with respect to the clean phase. The first interplanar spacing, for example, is contracted 5% with respect to the bulk. The buckling amplitudes on the third and fourth layer are 0.10 and 0.17 Å, respectively. The present work predicts an energy of −0.77 eV/(surface atom) for the monohydride surface, with respect to the clean (100)-(2×1) surface plus H_2 molecules. This indicates that hydrogen adsorption on the clean surface is energetically favorable.

Recent calculations, using the Car-Parinello method, indicated that the bare and monohydride terminated surfaces relaxed to (2×1) type reconstructed surface.[50] The reconstruction we obtain for the clean and monohydride phase are similar to what they obtained. Tsuda *et al.* employed an *ab initio* quantum chemistry method to study clean diamond (100)-(2×1) surface and predict a CC bondlength of about 1.39 Å.[51] Jing and Whitten used a quantum mechanical cluster method to study reconstruction on the clean (100) diamond surface.[18] They similarly found a (2×1) reconstruction and their results predict a CC dimer bondlength of about 1.401 and 1.508 Å, employing Hartree-Fock level and configuration-interaction (CI) calculations, respectively. Our bare C(100) CC bondlength (1.36 Å) is close to the CC bond distance predicted by Tsuda and co-workers and to the Hartree-Fock level calculation by Jing and Whitten. The calculated CC bondlength in the present work is not close to the result obtained by Jung and Whitten using the CI calculation (1.36 versus 1.508 Å), and may be due to the different model surface and basis sets employed.

2. *Electronic properties*

The surface electronic structure of the reconstructed (100) surface is illustrated in Fig. 8. Its salient features are (i) the presence of occupied and empty surface states associated with bonding and antibonding p_z orbitals of the surface dimers; (ii) at the Γ point, the surface bands splitting is ∼ 2.6 eV; (iii) a gap between these bands at the zone edges J and J'' (from zone center along and perpendicular to the surface C-C bond, respectively) caused by dimerization; (iv) interaction between the surface dimers introduces dispersion of the surface states along the J'' direction; and (v) for $\vec{k}$ lying between J'' and Γ, we find near degeneracy of the highest occupied (HO) state with the bulk valence edges states accompanied by partial delocalization of the HO wave function on the atoms on the third and fourth layers. Notice that these atoms, as mentioned above, have appreciable buckling amplitudes with respect to the bulk. The dispersion of the surface bands perpendicular to the dimers indicates that the dimer fragments are much more coupled to each other, relative to the surface chains in the Pandey (111) reconstructed surface. The carbons along the dimer row are closer compared to the distance of atoms between chains (2.5 Å versus 3.8 Å). The occupied bands are completely full and we see no crossing of the higher energy surface state to the Fermi level, indicating that the surface is not metallic. Photoemission measurements by Hamza *et al.*[14] for the (2×1) reconstructed diamond surface revealed occupied states in the gap and our calculated band structure clearly agrees with their results. The band structure of the monohydride phase, on the other hand, shows no state in the gap (see Fig. 8), which does not support the conclusion advanced by Gavrilenko to the contrary.[53] The surface that Gavrilenko dealt with may contain regions that are *not* hydrogen passivated and can give rise to the surface states he observed in the experiment. As pointed out in Ref. 20, the half-hydride

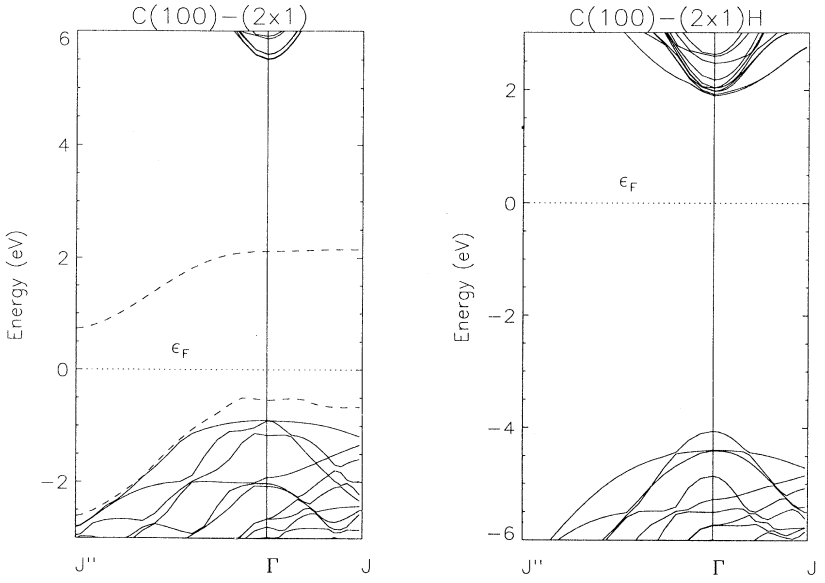

FIG. 8. Band structures for the clean and hydrogenated (2×1) reconstructed (100) surfaces of diamond. Dotted lines refer to the Fermi level, broken lines denote gap states. $J'' \rightarrow \Gamma$ is along the surface dimer CC bond, $\Gamma \rightarrow J$ is perpendicular.

surface may be a more ideal representation of the surface that Gavrilenko has investigated.

Shown in Fig. 9(a) is the simulated STM image for the clean (100) surface at energies E measured below the Fermi level. The isodensity surface of the bare surface is determined here using an energy interval of 0.1 eV centered at 0.6 eV below the Fermi energy (at the top of the occupied dangling state). The electron distribution profile at the highest occupied level of the clean surface shows a maximum on the C atoms, local minima along the CC bond and deeper minima between adjacent dimer rows. Figure 9(b) shows the calculated STM image for the monohydrogenated face. This plot is obtained using an energy interval of 0.1 eV at the top of the valence band. There appears to be a maximum along the CH bond and a minimum at the center of each dimer bond and a deeper minimum between adjacent dimer fragments. Unlike in the case of the clean surface, the simulated STM plot of the hydrogenated substrate shows a reduction of features on the surface dimer fragments, which is apparently caused by CH bond formation. Tsuno *et al.*[7] and Busmann *et al.*[23] reported STM investigations of their CVD grown (100) diamond surface and one of the main charteristics of their images is the presence of parallel "lines" at equal distance near terrace sites. They attributed these lines running along the dimer row direction, as dimer structures resulting from the (2×1) reconstruction. Our density profile also exhibits this main characteristic and yields strong support to the notion that these experimentally observed parallel lines are due to surface dimer structures. The limited resolution of the STM images, however, precludes us from making any conclusions as to whether the dimer structures they observed are hydrogenated or not.

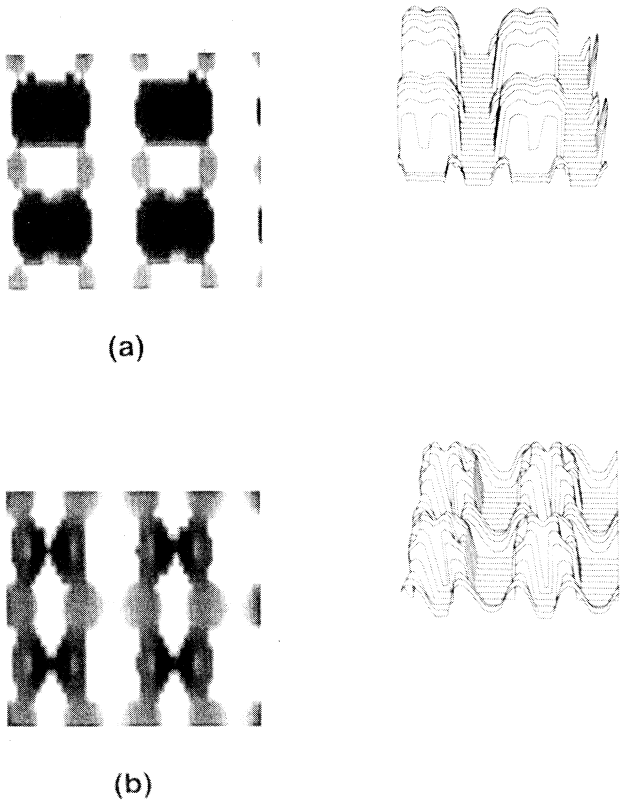

FIG. 9. Simulated STM images of the (a) clean and (b) hydrogenated (2×1) reconstructed (100) surfaces of diamond. Plots are drawn at isodensity $\rho \sim 0.01$ e/Å^3.

3. *Phonons*

The calculated surface phonon spectra of the clean and hydrogenated C(100)-(2×1) surfaces are shown in Fig. 10. As before these spectra represent the projected VDOS of the three upper C layers and three upper C layers plus surface H of the clean and H-terminated phase, respectively. Our predicted spectra is in good agreement with the HREELS results of Lee and Apai[10] and Aizawa *et al.*,[11] for both C(100)-(2×1) and C(100)-(2×1) surfaces as briefly presented previously.[24] We will therefore only review here the main features, provide schematic illustrations of the interesting phonon modes and focus our discussion on the comparison between the bare and hydrogenated surfaces spectra.

For the clean reconstructed surface, we have identified various excitations associated with the surface dimers (see Table I in Ref. 24). These vibrations can be characterized as dimer stretch, swing, rock, twist, and bounce modes. Except for the stretch modes, whose vibrations are nearly localized to the surface dimers, the other modes are coupled strongly to the subsurface excitations and between adjacent dimers producing frequencies depending on whether the dimer fragments move in or out of phase. For the H-terminated case, we observe excitations arising from the surface CH and CH-CH fragments. Several of these vibration motions are illustrated in Fig. 11.

Compared to the clean surface phonon spectrum, the hydrogenated phase has a distinct feature at the high frequency end of the spectrum (see Fig. 10). This band centered at 2730 cm^{-1}, due to localized surface CH stretching modes, as seen from the inspection of the eigenvectors associated with these features. Both spectra have bands below $\sim$ 1500 cm^{-1}. The clean (100) spectrum, however, has several broad weak features near 1489 cm^{-1}, which is identified as localized C-C stretching mode [see Fig. 11(a)]. It is interesting to note that this frequency lies in between the CC stretching frequency of singly bonded ethane (C_2H_6) and doubly bonded ethylene (C_2H_4), which are 995 and 1623 cm^{-1}, respectively. This fact together with the electronic band structure for the dimerized (100) surface, and the calculated CC dimer bondlength are strong indications that the bond order of the surface dimer is intermediate. Analogous CH-CH stretching modes were found for the hydrogenated case, although they are softer and coupled to subsurface excitations giving rise to splitting in the region 900–980 cm^{-1}. The band in the region 1000–1500 cm^{-1} is broader compared to the clean (100) spectrum. This region is dominated by surface H bending modes, such as H rocking or swing vibrations [see for example, Figs. 11(j)–(m)].

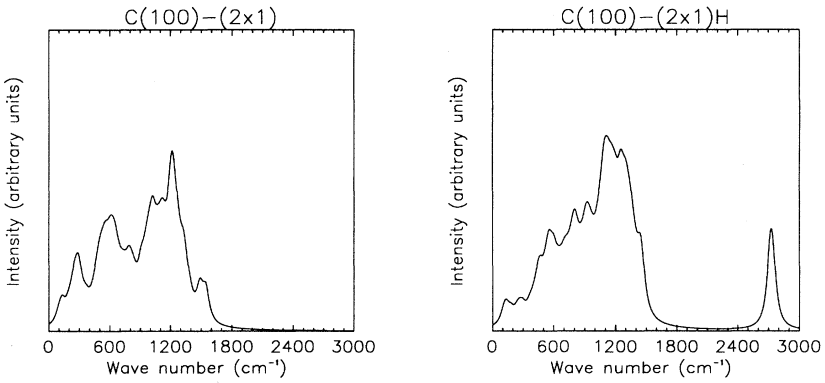

FIG. 10. Vibrational density of states of the clean and hydrogenated (100)-(2×1) surfaces of diamond.

C. Diamond (110) surface

1. *Structures*

The diamond (110) surface is composed of layers of zigzag chains, which resembles the surface chain of the C(111)-(2×1) structure, although the staggered stacking continues throughout the slab in this case. It is the least studied among the low-index planes of diamond. In this section, we discuss the properties of this surface as predicted from first-principles calculations. Low energy electron diffraction measurements of the as-polished surface show a (1×1) pattern similar to the structure of the truncated bulk.[6] Moreover, it was found that unlike the clean C(100) and C(111) substrates, the bare (110) surface exhibits no reconstruction even when annealed to over 1300 K.[6] To model the clean diamond (110) surface (C(110)), we relaxed our simulation system until it reached its minimum energy structure. The clean (110) slab is terminated with H on the top to model the hydrogenated (110) phase (C(110)H) and also relaxed to its minimum energy configuration using the *ab initio* techniques described previously. A representation of the C(110) and C(110)H surface are illustrated in Figs. 12(a) and 12(b).

Table IV summarizes the relaxed geometries of the C(110) and C(110)H surfaces. No reconstruction of the C(110) surface is found at $T = 0$ K, and it maintains a truncated bulk-like structure, in agreement with experiments.[6] The C-C bondlength of the first layer chain is about 1.44 Å, comparable to the graphite C-C bondlength of 1.42 Å. Unlike the case of the C(111)-(2×1) surface, the surface zigzag chains are *tilted* out of the surface plane. The average value of the tilt (relative difference in the vertical position of the "high" and "low" atoms) is predicted to be $\Delta z = 0.14$ Å. The "high" and "low" atoms move inwardly from their bulk positions by an average of 0.09 and 0.25 Å, respectively. Our calculations reveal small charge transfers, which seem to be universal for semiconductor surfaces exhibiting buckled surface fragments (e.g., Si).[54] The second layer chain, on the other hand, is not buckled. The C-C bondlength is calculated to be about 1.51 Å, slightly smaller than the C-C bulk diamond bondlength of 1.57 Å. The carbons on the second layer sink to the lattice with uniform distance of about 0.1 Å. Distortions from the bulk positions were seen down to the *seventh layer*. Terminating the surface with H atoms removes the chain's buckled configuration. Formation of CH bonds increases the first layer C-C bondlength to 1.54 Å and causes the atoms to move uniformly inwards by about 0.1 Å from their bulk position. The C-H bond is 1.17 Å and pointed away from the surface normal by about 29°. The first interplanar spacing is comparable to the bulk interplanar spacing, which is 1.26 Å. H adsorption on the C(110) surface is predicted to be energetically favorable; the hydrogenated face is stable by about 0.58 eV/(surface atom), relative to the clean (110) surface and the gas phase H_2 molecules.

TABLE IV. Structural properties for the relaxed (110) surfaces of diamond. $r_{1(C-C)}$ and $r_{2(C-C)}$ refer to the C-C bondlength in the first and second layer, respectively. Δz is the relative difference in the vertical position of the "high" and "low" atoms in the first layer chain, while r_{C-H} and Θ_{CH} are the surface C-H bondlength and its tilt with respect to the surface plane, respectively. The value in parentheses refers to the result from tight-binding calculations of Davidson and Pickett (see Ref. 20).

	C(110)-(2×1)	C(110)-(2×1)H
$r_{1(C-C)}$ (Å)	1.44 (1.43)	1.54 (1.52)
$r_{2(C-C)}$ (Å)	1.51 (1.49)	1.54 (1.53)
Δz (Å)	0.14 (0)	0 (0)
r_{C-H}		1.17 (1.124)
Θ_{CH} (deg)		29 (18.3)

2. *Electronic properties*

In Fig. 13, we show the calculated electronic surface bands for the bare (110) substrate. There are surface bands: one is filled and the other one is empty. At the zone center, the level splitting between the occupied and empty surface states is ~ 3.2 eV. Both the filled and empty surface bands have strong dispersion along Γ-J (parallel to the chain direction) and weak dispersion along J-K (perpendicular to the chains). In particular, the dispersion of surface electrons along the chains resembles nearly free electron behavior, with a gap at the zone edge, which is about 0.9 eV. The chains, on the other hand, are slightly coupled to each other, yielding a gap of about 1.5 eV at the K point. The minimum direct gap

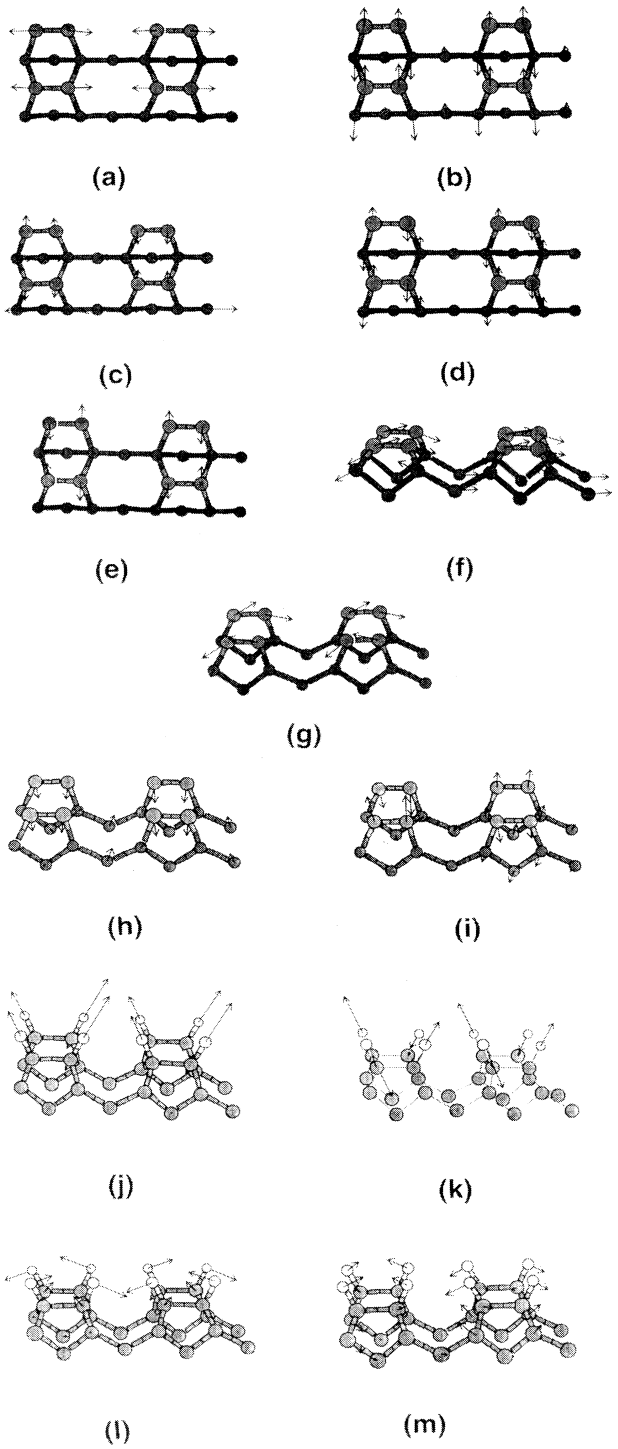

FIG. 11. Eigenvector representations of some of the phonon modes associated with the clean and hydrogenated (100)-(2×1) diamond surfaces: surface dimer (a) stretch, (b) swing (in phase), (c) swing (out of phase), (d) twist (in phase), (e) twist (out of phase), (f) rock (in phase), (g) rock (out of phase), (h) bounce (in phase), (i) bounce (out of phase), surface H (j) stretch (in phase), (k) stretch (out of phase), (l) rock (out of phase), and (m) scissoring motion. Carbon atoms appear shaded, hydrogen atoms white. Arrows show amplitudes for each atom in each mode.

($E_g = 0.9$ eV) occurs at J. Moreover, the C(110) surface is metallic; the higher energy surface states crosses the Fermi level.

The nonzero gap E_g between the filled and empty surface states is apparently caused by the asymmetry of the two atoms in the unit cell. The surface atoms along the zigzag chain relative to the subsurface are inequivalent and tilted. Comparison between the gap states of the C(110) surface and C(111)-(2×1) surface (see Figs. 13 and 2) shows their qualitative similarity. Notice that the top two layer chains of the C(111)-(2×1) surface resemble those of the C(110) surface. Both band structures yield an additional gap state near the conduction band, strong dispersion of the surface bands along the chain, and a weaker dispersion across the chains. The surface band, in the vicinity of the conduction band edge, resembles the bulk conduction band and is localized in the second layer chain. The coupling of the chains on the C(110) surface is stronger, however, [as evidenced by the larger surface bands dispersion across the neighboring chains of the C(110), relative to C(111)-(2×1)], since the chain fragments are ~ 0.8 Å closer, with respect to C(111)-(2×1) case. Moreover, notice that the gap at J point for the bare C(110) surface is bigger compared to the Pandey (111) reconstructed case. The main difference between the surface chain fragments in the two surfaces is that the (110) case is tilted. The further opening of E_g in the C(110) case can be related not only to the chain dimerization, but also to the zigzag chain tilt: this in-

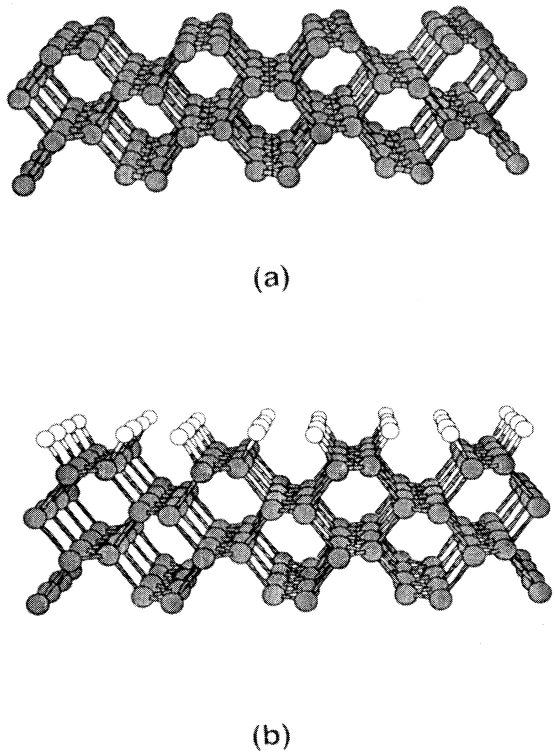

FIG. 12. Diagrams (side view) of (a) clean and (b) hydrogenated (110) surfaces of diamond. Carbon atoms appear shaded, hydrogen atoms white.

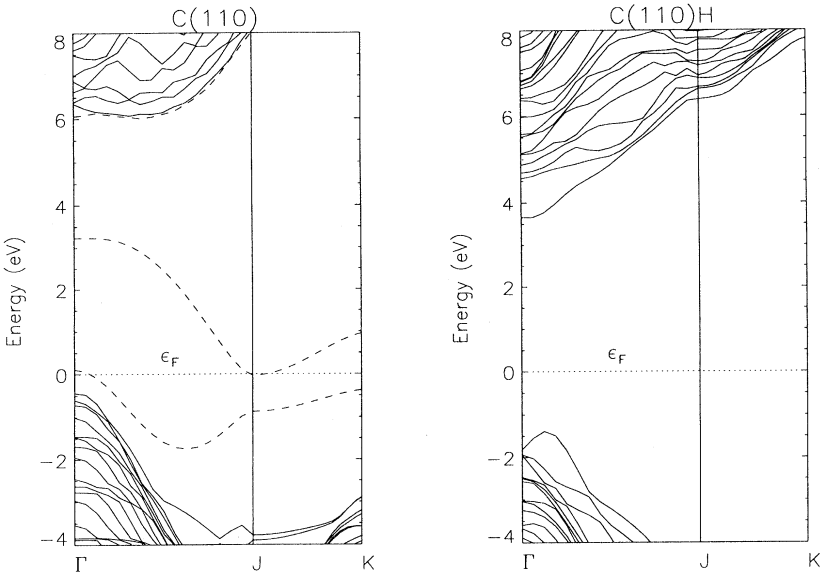

FIG. 13. Band structures for the clean and hydrogenated (110) surfaces of diamond. Dotted lines refer to the Fermi level, while broken lines denote gap states. $\Gamma \rightarrow J$ is along the chain direction, $J \rightarrow K$ is perpendicular.

crease in the gap shifts the band structure energy and drives the charge transfer.

The bare C(110) surface exhibits surface states in the gap, as shown in Fig. 13. This is consistent with the photoemission data of Pepper, which indicates the presence of gap states on the unhydrogenated (110) surface.[15] Moreover, photoemission experiments also reveal that once the (110) surface is hydrogenated, the gap states disappear.[15] Our electronic structure for the C(110)H substrate, as shown in Fig. 13, yielded no surface states, in agreement with the experiment.

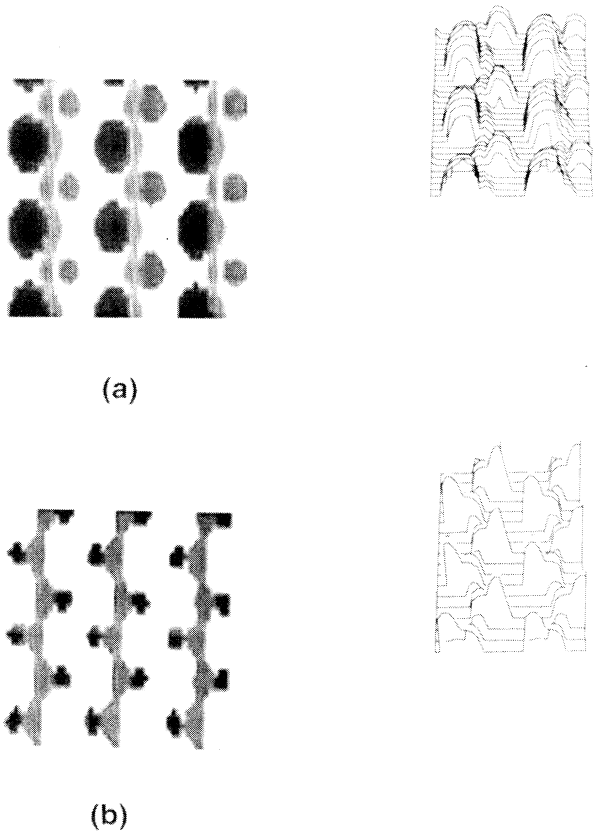

FIG. 14. Simulated STM images of the (a) clean and (b) hydrogenated (110) surfaces of diamond. Plots are drawn at isodensity $\rho \sim 0.01$ e/Å^3.

Figure 14 shows the simulated STM images of the C(110) and C(110)H surfaces. The isodensity surface for the bare surface in Fig 14(a) is determined using an energy interval of $\sim$ 0.5 eV centered near the Fermi energy. The plot in Fig. 14(b) for the C(110)H is obtained using an energy interval of 0.1 eV at the top of the valence band. The isodensity profile for the C(110) surface has maxima corresponding to the position of the "high" atoms with the feature on the "low" atoms appearing less pronounced. This is consistent with earlier findings that the surface chain of the C(110) surface is buckled. There are also features in between the "high" and "low" atoms giving rise to a zigzaglike pattern, a signature of the surface chain fragments. In contrast, the simulated STM image of the C(110)H substrate shown in Fig. 14(b) has a profile with maxima along the CH bonds. Minima appear along the surface chain fragments, and a deeper minimum between the zigzag chains. Presently, no STM measurements on the (110) surface are reported. We look forward to a comparison between future measurements and the present work.

3. Phonons

The surface phonon spectra for the C(110) and C(110)H surfaces are shown in Fig. 15. Similar to the spectra of the C(111)-(2×1) and C(100)-(2×1) surfaces, a mode-broadening Lorentzian of width 40 cm^{-1} is used to mimic experimental resolution. The phonon spectrum shown represents the projected VDOS of the three upper layers of the model C(110) surface, while the spectrum for the C(110)H substrate includes the surface H as be-

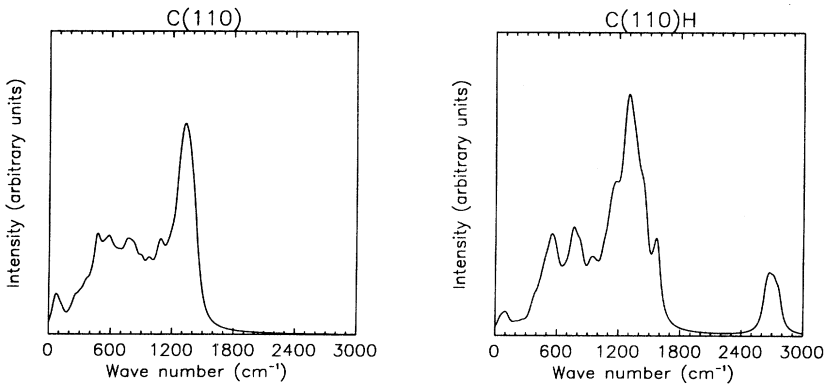

FIG. 15. Vibrational density of states of the clean and hydrogenated (110) surfaces of diamond.

fore. The spectrum for the clean surface exhibits features below $\sim$ 1500 cm^{-1}, with broadbands near $\sim$ 400–1000 cm^{-1} and $\sim$ 1000–1500 cm^{-1}. In the case of the C(110)H spectrum, additional bands are seen in the region 1400–1600 cm^{-1} and the bands above $\sim$ 1000 cm^{-1} appear to be broader. Moreover, the C(110)H spectrum has a distinct broad peak centered at 2675 cm^{-1}. Comparison of the major features in the calculated spectra for all the clean surfaces considered in this work reveals qualitative similarity. This observation also applies as one compares the characteristic features of the predicted vibrational spectra of the hydrogenated (100), (111), and (110) surfaces.

Various phonon modes associated with excitation of the first and second layer zigzag chains were identified for the clean (110) surface. These types of motion resemble those found in the surface fragments of the C(100)-(2×1) and C(111)-(2×1) surfaces, and they involve bouncing, rocking, and dimerization (dimer mode) of the C(110) chain structures. Notice that if these chain structures were not bonded to the lattice, the dimer mode would be the sole vibration mode available. We find vibrations highly localized to either the first layer or the second layer chain. The excitation involving the second layer zigzag chain lies at a higher energy, being relatively stiffer due to a higher coordination environment. The vibrational motion of the adjacent chains couple also, resulting in frequency splitting determined by the phase relationship of displacements on the neighboring chains. Table V summarizes the phonon modes associated with the surface chain structures, where adjacent chains undergo in-phase and out-of-phase motion. Several of these modes are schematically illustrated in Fig. 16. Notice that no prominent vibration which involves a clear rocking motion of the first layer chain is identified, unlike in the C(111)-(2×1) surface. The absence of this mode may be due to the buckled configuration of the C(110) chain structures, which then induces strong mixing with the lattice modes.

Termination of the C(110) surface with H atoms gives rise to vibrations involving the adsorbed H atoms. These motions are identified as stretching and bending motions of the CH fragments. We found that the region between 1000–1600 cm^{-1} is dominated by bending vibrations of the H atoms, which are coupled with lattice excitations. The CH bending motion interacts strongly, giving rise to symmetric and antisymmetric vibrations [see Fig. 16(i)–(l)]. The distinct peak near 2675 cm^{-1} is due to localized surface CH stretching motions. This CH stretch peak appears to be broader than those found in phonon spectra

TABLE V. Sample calculated frequencies and the corresponding description of surface-vibrational modes associated with the chain fragments of C(110) and C(110)H surfaces. The phase refers to the motion of the neighboring zigzag chain fragments.

Frequency (cm^{-1})	Description	Fig. 16
	C(110)	
412	surface chain bounce (out of phase)	a
537	surface chain bounce (in phase)	b
872	subsurface chain rock (in phase)	c
962	subsurface chain rock (out of phase)	d
1263	surface chain dimer mode (in phase)	e
1281	surface chain dimer mode (out of phase)	f
1405	subsurface chain dimer mode (out of phase)	g
1416	subsurface chain dimer mode (in phase)	h
	C(111)H	
2765	CH stretch (symmetric)	i
2635, 2644, 2758	CH stretch (antisymmetric)	j, k
$\sim$ 1000–1600	CH bend	l

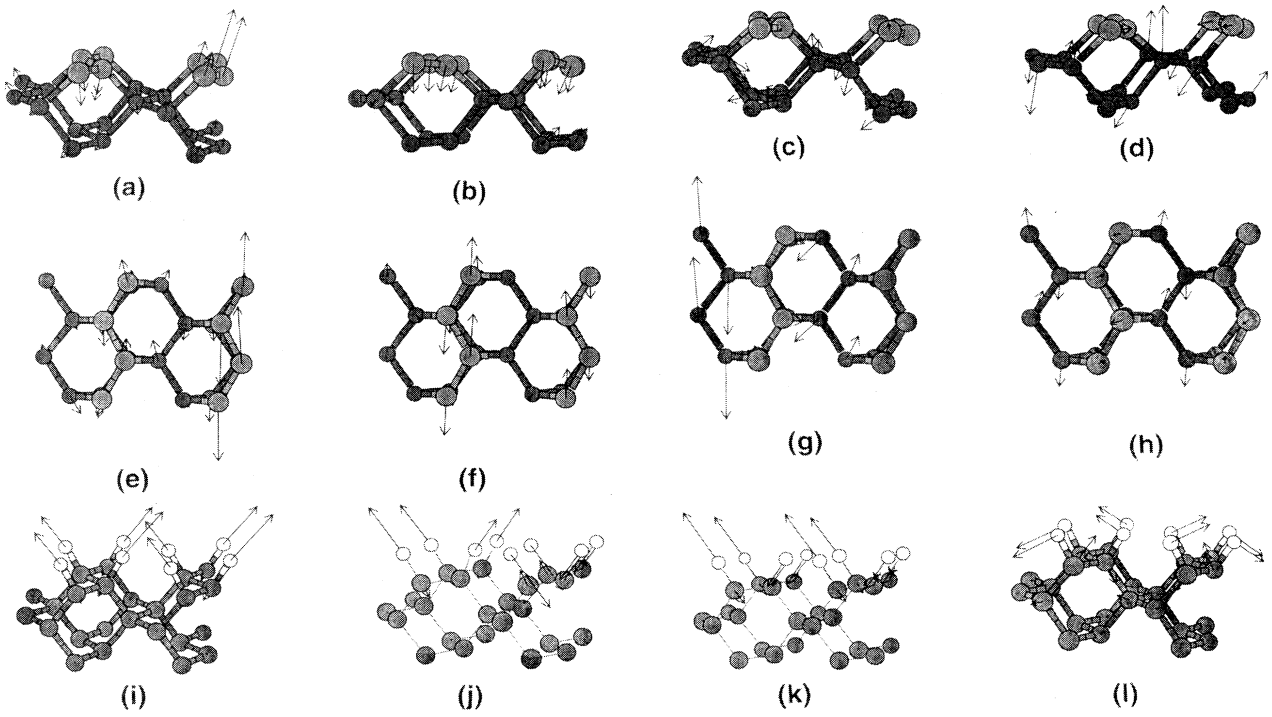

FIG. 16. Diagrammatic representations of some of the phonon modes associated with the clean and hydrogenated (110) diamond surfaces: (a) surface chain bounce (out of phase), (b) surface chain bounce (in phase), (c) subsurface chain rock (in phase), (d) subsurface chain rock (out of phase), (e) surface chain dimer mode (in phase), (f) surface chain dimer mode (out of phase), (g) subsurface chain dimer mode (out of phase), (h) subsurface chain dimer mode (in phase), surface H (i) stretch (symmetric) (j),(k) stretch (antisymmetric), and (l) bend. Carbon atoms appear shaded, hydrogen atoms white. Arrows show amplitudes for each atom in each mode.

of the C(100)-(2×1)H and C(111)-(1×1) surfaces. Inspection of the eigenvectors reveals that the H stretch modes are highly coupled, giving rise to several modes, which differ in the phase relationship of stretch motion of the neighboring H atoms. This wider splitting of the H stretch modes is due to smaller distance and, therefore, stronger interaction between the nearest neighbor surface H atoms, compared to the hydrogenated (100) and (111) cases.

IV. CONCLUSIONS

We have employed *ab initio* techniques to study the minimum energy configurations, electronic structures, and phonon modes of diamond (100), (111), and (110) surfaces. The clean (100) surface yielded a stable (2×1) reconstructed structure, while the (111) Pandey chain reconstructed structure is energetically favorable over the bulk-terminated (111) substrate. Unlike the clean (100)-(2×1) and Pandey (111) reconstructed surfaces, the surface fragments in the bare (110) surface is predicted to be buckled and accompanied by slight charge transfers between the "high" and "low" atoms. The H-terminated phases of the surfaces are energetically favorable compared to the corresponding clean surfaces plus H_2 molecules, as intuitively expected.

The surface electronic structures were also determined. All the unhydrogenated surfaces studied in the present investigations yielded gap states in the band structures, while passivation of the surfaces with H atoms remove the surface bands. The electronic band structures of the bare (110) and Pandey (111) reconstructed surfaces show qualitative similarity. Analysis of the dispersion of the surface states reveal interaction between the adjacent surface dimers in the clean (100)-(2×1) and neighboring zigzag chains in the bare Pandey (111) and (110) surfaces. We have also plotted within 0–2 eV of the Fermi level, isodensity profiles surfaces of the highest occupied surface states at a constant density to simulate STM images, and our results provide qualitative explanations of some features observed in the STM images of the as-grown (100) and (111) diamond surfaces.

The projected vibrational density of states of the clean surfaces yielded phonon modes involving excitations of the surface dimers and zigzag chains. In general, the vibrations of the neighboring surface fragments are coupled, giving rise to motions determined by phase displacements of the adjacent surface dimers or chains. Comparison of all the calculated phonon spectra for various clean diamond surfaces considered in the present work yielded gross features that are qualitatively similar. The calculated phonon spectra for the various H-terminated surfaces considered in this work have features associated with high frequency surface CH stretching modes. Except for the hydrogenated (111) bulk terminated substrate, the CH stretching motions are coupled giving rise to symmetric and antisymmetric vibrations. Modes due to CH bending vibrations were also identified for the various hydrogenated surfaces.

ACKNOWLEDGMENTS

We are indebted to D.W. Brenner for providing us with spline routines we use in the semiclassical calculations. Helpful discussions with M. Kordesch and S. Yang are appreciated. We thank the Minnesota Supercomputer Center for the Xmol graphic program. One of us (D.A.D.) acknowledges partial support from NSF Grant No. DMR-93-22412. D.R.A. thanks Ohio University for financial support.

[1] *Diamond and Diamond-Like Films and Coatings*, edited by R.E. Clausing, L.L. Hostou, J.C. Angus, and P. Koidl (Plenum, New York, 1991).
[2] *Proceedings of the Third International Symposium on Diamond Materials*, edited by J.P. Dismukes and K.V. Ravi, (The Electrochemical Society, New Jersey, 1993), Vol. 93, p. 17.
[3] See, for example, J.C. Angus and C.C. Haymann, Science **241**, 913 (1988).
[4] M.W. Geis, H.I. Smith, J. Argoitia, J. Angus, G.H. Ma, J.T. Glass, J. Butler, J. Robinson, and R. Pryor, Appl. Phys. Lett. **52**, 2043 (1988); C.J. Chu, M. D'Evelyn, R.H. Hauge, and J.L. Margrave, J. Appl. Phys. **70**, 1695 (1991).
[5] For a review, see F.G. Celii and J.E. Butler, Ann. Rev. Phys. Chem. **42**, 643 (1991).
[6] P.G. Lurie and J.M. Wilson, Surf. Sci. **65**, 453 (1977).
[7] T. Tsuno, T. Imai, Y. Nishibayashi, K. Hamida, and N. Fujimori, Jpn. J. Appl. Phys. **30**, 1063 (1991).
[8] T. Fraunheim, U. Stephan, P. Blaudeck, D. Porezag, H.-G. Busmann, W. Zimmerman-Edling, and S. Lauer, Phys. Rev. B **48**, 18 189 (1993).
[9] F.J. Himpsel, D.E. Eastman, P. Heidmann, and J.F. Van der Veen, Phys. Rev. B **24**, 7270 (1981); T.E. Derry, L. Smit, and J.E. Van der Veen, Surf. Sci. **167**, 502 (1986).
[10] S. -Tong Lee and G. Apai, Phys. Rev. B **48**, 2684 (1993).
[11] T. Aizawa, T. Ando, M. Kamo, and Y. Sato, Phys. Rev. B **48**, 18 348 (1993).
[12] A.V. Hamza, G.D. Kubiak, and R.H. Stulen, Surf. Sci. Lett. **206**, L833 (1988).
[13] R.P. Chin, J.Y. Huang, Y.R. Shen, J.T. Chuang, H. Seki, and M. Buck, Phys. Rev. B **45**, 1522 (1992).
[14] A.V. Hamza, G.D. Kubiak, and R.H. Stulen, Surf. Sci. **227**, 35 (1990).
[15] S.V. Pepper, J. Vac. Sci. Technol. **20**, 213 (1982).
[16] S.V. Pepper, Surf. Sci. **123**, 47 (1982).
[17] S. Iarlori, G. Galii, P. Gygi, M. Parinello, and E. Tosatti, Phys. Rev. Lett. **69**, 2947 (1992).
[18] Z. Jing and J.L. Whitten, Phys. Rev. B **50**, 2598 (1994).
[19] S.H. Yang, D.A. Drabold, and J.B. Adams, Phys. Rev. B **48**, 5261 (1993).
[20] B.N. Davidson and W.E. Pickett, Phys. Rev. B **49**, 11 253 (1994).
[21] D.R. Alfonso and S.E. Ulloa, Phys. Rev. B **48**, 12 235 (1993); D.R. Alfonso, S.E. Ulloa, and D.W. Brenner, *ibid.* **49**, 4948 (1994).
[22] M.S. Melnik, D.G. Goodwin, and W.A. Goddard (unpublished).
[23] H.-G. Busmann, W. Zimmermann-Edling, H. Sprang, H.J. Guntherodt, and I.V. Hertel, Diamond Relat. Mater. **1**, 979 (1992).
[24] D.R. Alfonso, D.A. Drabold, and S.E. Ulloa, Phys. Rev. B **51**, 1989 (1995).
[25] O.F. Sankey and D.J. Niklewski, Phys. Rev. B **40**, 3979 (1989); O.F. Sankey, D.J. Niklewski, D.A. Drabold, and J.D. Dow, *ibid.* **41**, 12 750 (1990).
[26] G.B. Adams, O.F. Sankey, M. O'Keefe, J.B. Page, and D.A. Drabold, Science **256**, 1792 (1992).
[27] D.A. Drabold, P.A. Fedders, S. Klemm, and O.F. Sankey, Phys. Rev. Lett. **67**, 2179 (1991); D.A. Drabold, R. Wang, S. Klemm, and O.F. Sankey, Phys. Rev. B **43**, 5132 (1991).
[28] J. Harris, Phys. Rev. B **31**, 1770 (1985).
[29] F. Herman and S. Skillman, *Atomic Structure Calculations* (Prentice-Hall, Englewood Cliffs, NJ, 1963).
[30] D.M. Ceperley and G.J. Alder, Phys. Rev. B **23**, 5048 (1981).
[31] J. Perdew and A. Zunger, Phys. Rev. B **23**, 5048 (1981).
[32] D.A. Drabold, P. Stumm, and P.A. Fedders, Phys. Rev. Lett. **72**, 2666 (1994); D.A. Drabold, P.A. Fedders, and P. Stumm, Phys. Rev. B **49**, 16 415 (1994).
[33] H.J. Monkhorst and J.D. Pack, Phys. Rev. B **13**, 5188 (1977).
[34] D.W. Brenner, Phys. Rev. B **42**, 9458 (1990).
[35] D.R. Alfonso, S.H. Yang, and D.A. Drabold, Phys. Rev. B **50**, 15 369 (1994).
[36] J. Tersoff and D.R. Hamann, Phys. Rev. Lett. **50**, 1998 (1993).
[37] G. Vidali and D.R. Frankl, Phys. Rev. B **37**, 2480 (1983).
[38] B.B. Pate, Surf. Sci. **83**, 161 (1986).
[39] K.C. Pandey, Phys. Rev. B **25**, 4338 (1982).
[40] D. Vanderbilt and S.G. Louie, Phys. Rev. B **29**, 7099 (1984).
[41] R. Stumpf and P.M. Marcus, Phys. Rev. B **47**, 16 016 (1993).
[42] X. Zhu and S.G. Louie, Phys. Rev. B **45**, 3940 (1992).
[43] K.A. Killian, D.A. Drabold, and J.B. Adams, Phys. Rev. B **48**, 17 393 (1993).
[44] G.D. Kubiak and K.W. Kolasinski, Phys. Rev. B **39**, 1381 (1989).
[45] H.-G. Busmann, W. Zimmermann-Edling, S. Lauer, Th. Fraunheim, P. Blaudeck, and D. Porezag, Surf. Sci. **295**, 340 (1993).
[46] O.L. Alerhand and E.J. Mele, Phys. Rev. B **37**, 2536 (1988).
[47] B.D. Thoms, P.E. Pehrsson, and J.E. Butler, J. Appl. Phys. **75**, 1804 (1994).
[48] B.J. Waclawski, D.T. Pierce, N. Swanson, and R.J. Celotta, J. Vac. Sci. Technol. **21**, 368 (1982).
[49] B. Sun, X. Zhang, Q. Zhang, and Z. Lin, Appl. Phys. Lett. **62**, 31 (1993).
[50] J. Weide, Z. Zhang, P.K. Baumann, M.G. Wensell, J. Bernholc, and R.J. Nemanich, Phys. Rev. B **50**, 5803 (1994).
[51] M. Tsuda, S. Oikawa, S. Furukawa, C. Sekine, and M. Hata, J. Electrochem. Soc. **139**, 1482 (1992).
[52] I.N. Levine, *Physical Chemistry*, 3rd ed. (McGraw-Hill, New York, 1988).
[53] V.I. Gavrilenko, Phys. Rev. B **47**, 9556 (1993).
[54] See, for example, P. Bogulawski, Q.M. Zhang, Z. Zhang, and J. Bernholc, Phys. Rev. Lett. **72**, 3694 (1994).

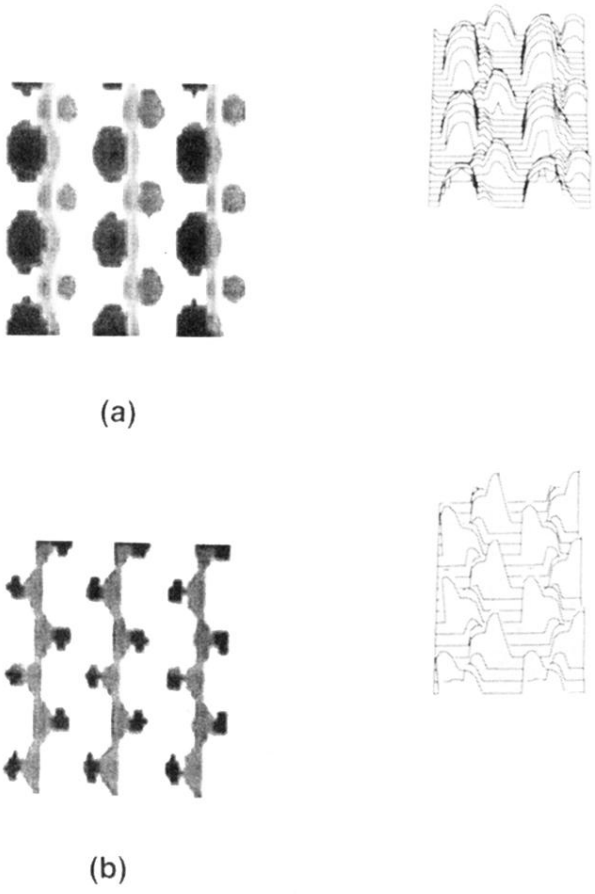

FIG. 14. Simulated STM images of the (a) clean and (b) hydrogenated (110) surfaces of diamond. Plots are drawn at isodensity $\rho \sim 0.01$ e/Å^3.

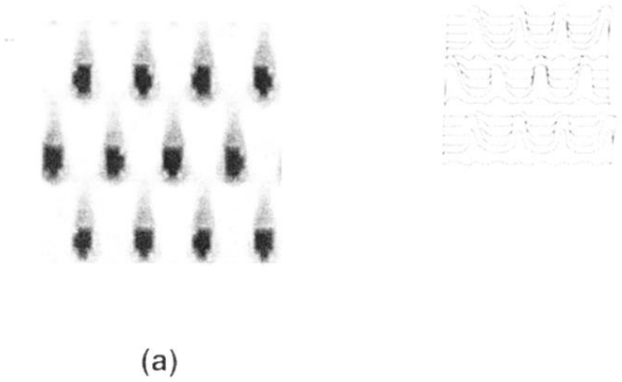

FIG. 4. Simulated STM images of the (a) hydrogenated bulk terminated and (b) Pandey chain (2×1) reconstructed (111) surfaces of diamond. Plots are drawn at isodensity $\rho \sim 0.01$ e/Å^3.

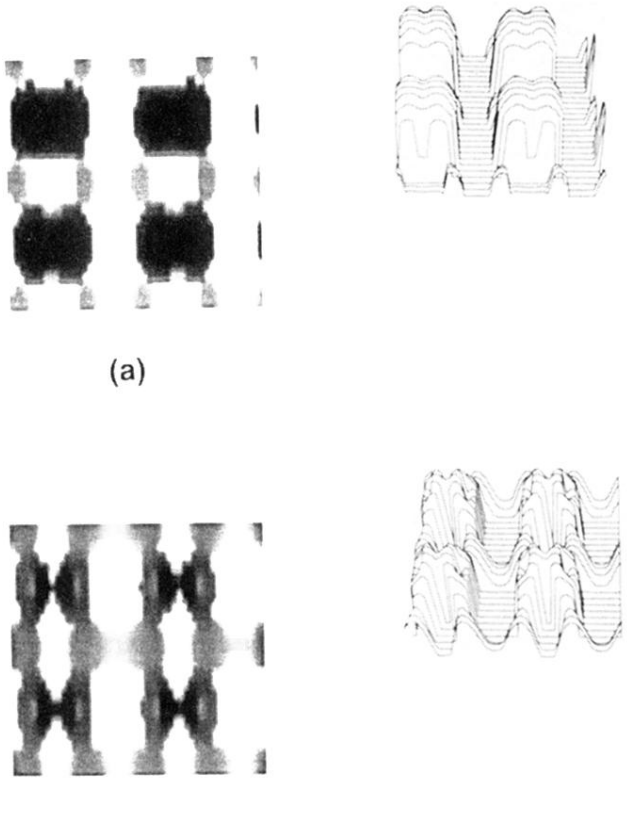

FIG. 9. Simulated STM images of the (a) clean and (b) hydrogenated (2×1) reconstructed (100) surfaces of diamond. Plots are drawn at isodensity $\rho \sim 0.01$ e/Å^3.